
Article:
Wilkes, M.D. and Brown, S. orcid.org/0000-0001-8229-8004 (2022) Flexible CO2 capture for open-cycle gas turbines via vacuum-pressure swing adsorption : a model-based assessment. Energy, 250. 123805. ISSN 0360-5442

https://doi.org/10.1016/j.energy.2022.123805

Energy 250 (2022) 123805

Contents lists available at ScienceDirect

Energy

journal homepage: www.elsevier.com/locate/energy

Flexible CO_2 capture for open-cycle gas turbines via vacuum-pressure swing adsorption: A model-based assessment

Mathew Dennis Wilkes, Solomon Brown*

Department of Chemical and Biological Engineering, University of Sheffield, Sheffield, S1 3JD, United Kingdom

ARTICLE INFO

Article history:
Received 2 December 2021
Received in revised form
16 March 2022
Accepted 19 March 2022
Available online 22 March 2022

Keywords:
CO_2 adsorption
Dynamic modelling
Post-combustion capture
Flexible operation
VPSA

ABSTRACT

As energy systems require flexible and responsive power generators to combat network imbalances, CO_2 post-combustion capture (PCC) technologies need to be capable of transient operation. However, currently only amine absorption has been investigated for its efficacy in Flexible-PCC.

Within this study we develop and validate a vacuum-pressure swing adsorption (VPSA) process model, capable of processing 33.8 kg/s of exhaust flow from a small-scale open-cycle gas turbine (OCGT). The Flexible response scenario is based on realistic load changes of OCGTs during a 5-h period. To handle the size of flow the system is split into two identical two bed four step VPSA processes, both using Zeolite 13X as the adsorbent material. Included in the Flexible-VPSA operation is the start-up, ramping, and shutdown procedures. Flexible-VPSA showed minute deviations in CO_2 purity and recovery rate, and despite the specific energy demand increasing, results show no technical limitations to transient operation. The Flexible VPSA simulations are compared against the benchmark MEA solvent, with both technologies performing similarly when processing highly transient flue gas flowrate. Thus, VPSA is potentially an attractive alternative technology for Flexible-PCC.

1. Introduction

With the realistic constraints (peak demand, system inertia and capacity reserve requirements) put on the energy system due to an increased renewable capacity [1], the use of Carbon Capture Utilisation and Storage (CCUS) for fossil-based power generation focusses on flexible operation [2]. System flexibility is crucial in counteracting fluctuations in supply and demand, balancing the network and maintaining security of supply [3]. However, the majority of Flexible-CCUS literature revolves around post-combustion capture (PCC) via amine absorption [4–8], as this is considered the benchmark CO_2 capture technology [9].

Physical adsorption is a promising alternative and is advantageous because no new bond is formed, enabling the possibility of pressure, temperature or vacuum swing regeneration at a much lower cost compared to amine-absorption. Several physical adsorbents have been extensively researched: zeolites, metal organic frameworks (MOFs), silicas, and carbonaceous material [10–14]. Ben-Mansour et al. [13] provide an extensive review of physical adsorption and discuss various regeneration processes. The study highlights fixed bed pressure swing adsorption (PSA) as an economic option because of its comparatively simple application, low energy demand, and low investment cost. For PCC vacuum swing adsorption (VSA) is attractive as the feed stream is at atmospheric (or slightly elevated) pressure. However, PSA/VSA systems suffer scalability issues and multiple beds are required to deliver the specifications for downstream compression equipment [9]. With the relatively low thermal regeneration temperatures, and the availability of waste heat from the flue gas, Zanco et al. [15] suggests the more effective option would be temperature swing adsorption (TSA). In the literature high purities and recovery rates can be obtained by combining processes, i.e. pressure-temperature swing adsorption (PTSA), vacuum-pressure swing adsorption (VPSA) or vacuum-temperature swing adsorption (VTSA) [16–20].

Only a small number of studies have presented pilot-scale data for CO_2/N_2 adsorption systems, shown in Table 1. Wang et al. [18] achieved >90% capture and >95% purity with a two-unit VPSA system. The energy consumption is a sum of the power demand from blowers and pumps in the pilot facility. The on-site Watt metres measured a power demand of 2.44–2.65 MJ/kgCO_2. Lower than the 3.6–4.0 MJ/kgCO_2 for amine-absorption using the benchmark 30 wt% monoethanolamine [9]. All the studies shown in

* Corresponding author.
E-mail address: s.f.brown@sheffield.ac.uk (S. Brown).

https://doi.org/10.1016/j.energy.2022.123805

Table 1
Pilot-scale studies of CO_2 adsorption from flue gas.

Source	System	Configuration	CO_2 Feed (%)	Feed Flowrate	Recovery (%)	Purity (%)	Energy Consumption
[35]	PTSA	First stage is a PTSA unit, second stage is a PSA unit, using a Ca-X type zeolite. Feed comes from a dehumidifier unit attached to Yokosuka Thermal Power Station (coal and oil fired)	11.5	1000 N m^3/h	90	99	560 kWh/t-CO_2
[36]	TSA	Single bed TSA system with simulated flue gas. Lab scale comparison of Zeolite 13 X and 5A	10	20 N m^3/min	13X = 65 5A = 83	13X = 94 5A = 98	8.8 MJ/kgCO_2 6.4 MJ/kgCO_2
[37]	VSA	Three bed VSA system using Zeolite 13X, evaluating the performance of 6 and 9 step cycles	8–22	66–115 L/min	6 step = 60-80 9 step = 60-70	6 step = 82-83 9 step = 90-95	6 step = 4–8 kW/tCO_2 9 step = 6–10 kW/tCO_2
[29]	VPSA	Three bed seven step VPSA unit removes CO_2 from an existing coal-fired power station using Zeolite 13X APG	15	32.1–45.9 Nm^3/h	79	85	2.37 MJ/kgCO_2
[18]	VPSA	The first unit is a 3 bed 8 step VPSA system using Zeolite 13X APG, the second unit is a 2 bed 6 step VPSA unit with activated carbon beads.	15–17	35.5–37.0 Nm^3/h	90.20	95.60	2.44 MJ/kgCO_2
[38]	VPSA	Single bed four step VSA with simulated flue gas feed for the basic system. Two bed four step VSA for the light product pressurisation (LPP) system. Both using Zeolite 13X	15	1000 SLPM	Basic: 95.9 ± 1 LPP: 94.8 ± 1	Basic: 86.4 ± 5.6 LPP: 89.7 ± 5.6	Basic: 472.2 ± 36.7 kWh/tonne CO_2 LPP: 475 ± 36.7 kWh/tonne CO_2
[39]	VPSA	Dual-Reflux VPSA in four fixed beds using two different activated carbon adsorbents within a single bed. Using a flue gas from a 460 MW CFB boiler.	11.1	100 N m^3/h	8 step: 42.7 9 step:30.2	8 step: 78.4 9 step: 89	8 step: 764 kWh/MgCO_2 9 step: 978 kWh/MgCO_2

Table 1 use fixed columns packed with an adsorbent material. Several studies have highlighted the potential for fluidised beds [21–23] and moving beds [24–26]. However, as the majority of CO_2 adsorption studies focus on fixed columns, this is the equipment investigated in this study. Table 2 is a compilation of simulation-based studies investigating CO_2/N_2 separation for PCC. As can be seen in Tables 1 and 2, Zeolite 13X is the most studied post-combustion CO_2 capture adsorbent, due to its high CO_2/N_2 selectivity and high adsorption capacity at low CO_2 partial pressure [26]. As a result, Zeolite 13X is the adsorbent material investigated in this study.

Jiang et al. [27] compared VPSA, TSA and TVSA configurations at lab-scale and found VPSA to be more effective due to a lower energy consumption and higher CO_2 productivity. VPSA systems have been investigated from lab-to pilot-scale [18,27–31] and usually comprise of two stages. The first stage captures >90% of the CO_2, and the second stage is used to increase the purity to >95% [32]. Luberti et al. [33] provides the design and simulation of a rapid VPSA process for PCC on a 10 MW_{th} biomass CHP plant. To handle the high flowrates and overcome scalability issues of adsorption process, in the 1st stage the flue gas stream is split into two parallel two-bed VPSA units, to capture >90% CO_2. The 2nd stage, another two-bed VPSA unit, is used for purification to obtain >95% CO_2.

Rui et al. [34] analysed CO_2 capture from flue gas using VPSA under unstable feed concentrations. The model-based study incorporated PID control strategies (closed-loop and open-loop feedback control) to adjust adsorption step duration for product quality control during variable feed concentration. To the authors knowledge, adsorption technologies for Flexible-CCUS have not previously been investigated.

In our previous study we highlighted the effects of transient open-cycle gas turbine (OCGT) operation on an amine-PCC system [7]. This study aims at investigating VPSA systems for quick response OCGTs (see Fig. 1), under the same transient flue gas input to enable a comparison with the benchmark PCC technology. Within this Flexible-VPSA study:

- Development and validation of a single column process model for a VPSA system for CO_2 capture from flue gas using Zeolite13X.
- Designing and scaling the process model for a small-scale OCGT.
- Analysis of system flexibility, i.e., under transient flue gas conditions.
- Comparison against the benchmark amine-PCC system.

2. Adsorption modelling

Throughout the literature, models are usually one-dimensional and axially dispersed, assuming plug flow regime and negligible temperature, pressure, and concentration variation in the radial domain. Li et al. [62] provides a literature review of mathematical models of carbon capture by adsorption (CCA). Fig. 2 illustrates the composition of physical adsorption model. The material balance over the fixed bed includes two important sub-models: adsorption kinetics (rate of mass transfer between gas and solid) and adsorption equilibrium (isotherm model). Table 2 highlights mathematical models in the literature specific for CO_2/N_2 adsorption. The Linear Driving Force (LDF) model is the most commonly used mechanism to describe mass transfer between the fluid and adsorbent, as it considers internal diffusional and external convection [71]. For CCA several isotherm models are commonly used in the literature, as highlighted in Table 2, usually an extension of the Langmuir isotherm model (dual-site Langmuir, Freundlich, Langmuir-Freundlich, BET, Sips, Toth) which account for multi-component mixtures. The Ideal Adsorption Solution (IAS) theory has also been used, utilising pure component adsorption isotherms and enabling different isotherm models to be used for each component [57,58,72,73].

The energy balance describes the heat transfer between the gas and solid particles, as well as the column wall. Mathematic models in the literature vary in complexity of their consideration of heat transfer. Non-isothermal and non-adiabatic models that account

Table 2
Compilation of studies presenting mathematical models of various adsorption-based PCC systems.

Source	Model					Adsorbent(s) Investigated	System
	Mass Transfer	Flow	Isotherm	Heat Transfer	Pressure Drop		
[40]	LDF	Axially dispersed plug flow regime	Langmuir	Thermal equilibrium	Negligible Pressure Drop	Activated Carbon and Zeolite 13X	PSA
[41]	LDF	Ideal plug flow	Langmuir	Isothermal conditions	Negligible Pressure Drop	Zeolite 13X, 5A, 4A	DAC PSA
[42]	LDF	Axially dispersed plug flow regime	Langmuir	Non-equilibrium	Ergun	Potassium promoted hydrotalcite	PSA
[43]	LDF	Ideal plug flow	Extended Langmuir	Non-isothermal Adiabatic conditions	Negligible Pressure Drop	Zeolite 13X	PSA
[44]	LEM	Axially dispersed plug flow regime	Langmuir	Non-isothermal	Negligible Pressure Drop	Zeolite 13X	VSA
[45]	LDF	Axially dispersed plug flow regime	Dual-site Langmuir	Non-isothermal	Ergun	Zeolite 13X	Fractionated VPSA
[46]	LDF	Axially dispersed plug flow regime	Dual-site Langmuir	Thermal equilibrium	Ergun	Zeolite 13X	PSA
[16]	LDF	Axially dispersed	Toth	Local thermal equilibrium	Darcy	Zeolite 5A	TSA
[47]	LDF	Axially dispersed plug flow regime	Toth	Non-equilibrium	Ergun	Activated Carbon	PSA
[48]	LDF	Axially dispersed plug flow regime	Toth	Non-equilibrium	Ergun	Zeolite 13X	PSA
[49]	LDF	Axially dispersed plug flow regime	Toth	Thermal equilibrium	Ergun	Zeolite 13X	PSA
[50]	LEM	Axially dispersed plug flow regime	IAS theory using dual-site Langmuir-Freundlich isotherm	Isothermal conditions	Negligible Pressure Drop	Zeolite 13X,Mg-MOF-74, MOF-177, CubTTri, BeBtB and Co(BDP)	Breakthrough analysis
[51]	LEM	Axially dispersed plug flow regime	IAS theory using dual-site Langmuir-Freundlich isotherm	Isothermal conditions	Negligible Pressure Drop	Zeolites (MFI, JBW, AFX, NaX) and Metal Organic Frameworks (MgMOF-74, MOF-177, CuBTTri-mmen)	PSA
[52]	LDF	Axially dispersed plug flow regime	Langmuir	Thermal equilibrium	–	Ceca 13X, Alcan AA320-AP and Alcan 650 PCA	TPSA
[30]	LDF	Axially dispersed	Virial	Non-equilibrium	Ergun	Activated Carbon Beads	VPSA
[17]	Bi-LDF	Axially dispersed plug flow regime	Modified multisite Langmuir	Thermal equilibrium	Ergun	Zeolite 13X-APG	VSA, TSA, VTSA
[53]	LDF	Axially dispersed plug flow regime	Multi-site Langmuir	Isothermal conditions	Ergun	activated carbon honeycomb monolith with zeolite 13X particle	ESA
[54]	LDF	Axially dispersed	Langmuir	Thermal equilibrium	Darcy	Zeolite 13X	VSA
[38]	LDF	Axially dispersed	Langmuir	Thermal equilibrium	Darcy	Zeolite 13X	VSA
[55]	LDF	Axially dispersed plug flow regime	Multi-site Langmuir	Thermal equilibrium	Ergun	Zeolite 5A and activated carbon	PSA
[56]	LDF	Axially dispersed	Toth	Non-equilibrium	Ergun	Zeolite 13X, Amine-functionalised Activated Carbon, Lewatit VP OC 1065	VSA
[57]	LDF	Axially dispersed	IAS theory using the Toth isotherm model	Thermal equilibrium	Ergun	Microporous Biochar	Ternary breakthrough analysis
[58]	LDF	Axially dispersed	IAS theory using Toth for CO_2 and N_2, CMMS theory for H_2O	Thermal equilibrium	Ergun	Microporous Biochar	Ternary breakthrough analysis
[33]	LDF	Axially dispersed plug flow regime	Langmuir	Thermal equilibrium	Ergun	Zeolite 13X	Rapid VPSA
[59]	LDF	Axially dispersed	Dual-site Langmuir	Thermal equilibrium	Ergun	Zeolite 13X and Mg-MOF-74	VPSA
[60]	LDF	Axially dispersed	IAS theory using Toth for CO_2 and N_2, CMMS theory for H2O	Non-equilibrium	Darcy	Activated Carbon Honeycomb	TSA
[61]	quasi-second order mass transfer	Axially dispersed plug flow regime	Toth	Isothermal conditions	Ergun	Activated Carbon and Zeolite 13X	VSA
[62]	LDF	Axially dispersed plug flow regime	Toth	Non-equilibrium	Ergun	Activated Carbon	PSA
[63]	LDF	2-D Mesh of structured quadrilateral elements	Dual-site Langmuir for CO_2 & N_2, Toth for H_2O	Thermal equilibrium	Ergun	Zeolite 13X and Mg-MOF-74	2D and 3D breakthrough analysis
[64]		Axially dispersed	Extended Langmuir	Non-isothermal and adiabatic	Karman-Kozeny	Zeolite MS13X and activated carbon honeycomb	T/ESA
[65]	LDF	2-D Mesh of structured quadrilateral elements	Toth model for Zeolite 13X and the dual-site Langmuir model for Mg-MOF-74	Thermal equilibrium	Ergun	Zeolite 13X and Mg-MOF-74	Breakthrough analysis

(*continued on next page*)

Table 2 (*continued*)

Source	Model					Adsorbent(s) Investigated	System
	Mass Transfer	Flow	Isotherm	Heat Transfer	Pressure Drop		
[66]	LDF	Axially dispersed plug flow regime	Langmuir	Thermal equilibrium	Darcy	Silica Gel	VSA
[26]	LDF	Axially dispersed	Extended Virial Isotherm	Non-equilibrium	Ergun	Zeolite 13X	MBTSA
[67]	LDF	Axially dispersed plug flow regime	Langmuir-Freundlich	Thermal equilibrium	Ergun	Nanostructured Zeolite pellets	VPSA
[68]	LDF	Axially dispersed	dual-site Langmuir isotherm	Thermal equilibrium	Ergun	Zeolite 13X	VSA
[27]	LDF	Axially dispersed	Extended Langmuir	Non-equilibrium	Ergun	Zeolite 13X	VPSA, TSA, TVSA
[69]	LDF	Axially dispersed	Extended Langmuir	Non-equilibrium	Ergun	Composite adsorption material	VPSA
[70]	LDF	Axially dispersed	Sips	Thermal-equilibrium	Ergun	Zeolite-geopolymer sorbent	TSA-PSA

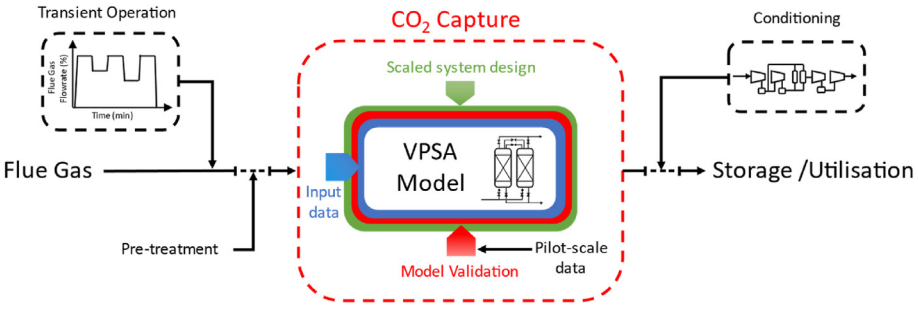

Fig. 1. Study overview looking at VPSA CO_2 capture from transient flue gas, only the aspects within the red dotted border are investigated within this study.

for heat transfer between the gas and solid adsorbent, are classified as non-equilibrium models. Those that consider the energy flux between the gas and solid adsorbent as negligible are in thermal equilibrium [62]. The momentum balance considers the pressure drop in the column due to resistances in gas flow, modelled using the Blake-Kozeny equation (linear-laminar flow), the Ergun equation (non-linear turbulent flow) or the Darcy equation [71].

2.1. Process simulation

The process model used in this work (single column used for validation and multi-column used for large-scale dynamic analysis) is one dimensional and axially dispersed, with fluid flow described through the plug flow model, i.e., no radial variation in temperature, pressure, and concentration. The fluid phase material balance for component *i* through the packed bed is represented by the axial plug flow model [72]:

$$-D_L\frac{\partial^2 C_i}{\partial z^2}+\frac{\partial}{\partial z}(v_s C_i)+\frac{\partial C_i}{\partial t}+\left(\frac{1-\varepsilon}{\varepsilon}\right)\frac{\partial \overline{q_i}}{\partial t}=0,\ \forall i\in Components,\ \forall z\in(0,L) \quad (1)$$

where D_L is the axial dispersion coefficient [m^2/s], C_i is the fluid component concentration [kmol/m^3], z is the distance along the axial direction [m], L is the bed length [m] v_s is superficial fluid velocity [m/s], and ε is the bed voidage. Assuming axial flow is from the feed to the product side of the adsorption column, the boundary conditions are:

$$\frac{F^{in}w_i^{in}}{A_{bed}}=v_s C_i-\varepsilon D_l\frac{\partial C_i}{\partial z},\ \forall i\in Components, z=0 \quad (2)$$

$$\varepsilon D_l\frac{\partial C_i}{\partial z}=0,\ \forall i\in Components,\ z=L \quad (3)$$

where F^{in} is the molar flowrate entering the bed [kmol/s], w^{in} is the component molar fraction [kmol/kmol], and A_{bed} is the bed cross-sectional area [m^2]. The mass transfer rate is described through the LDF model [74]:

$$\frac{\partial \overline{q_i}}{\partial t}=k\left(q_{eq,i}-\overline{q_i}\right),\ \forall i\in Components \quad (4)$$

where $\overline{q_i}$ is the averaged absorption amount of species *i* [kmol/kg], $q_{eq,i}$ is the equilibrium absorption amount of species *i* [kmol/kg], and *k* is the mass transfer coefficient [1/s]. The dual-site Langmuir

isotherm model was chosen as this is commonly used in the literature [38,45,59,68,75,76]. The dual-site Langmuir isotherm is non-competitive as N_2 adsorption is low and does not significantly affect the adsorption amount of CO_2 [77], it calculates the equilibrium adsorption amount [38]:

$$q_{eq,i} = \frac{q_{sb,i} b_i C_i}{1 + b_i C_i} + \frac{q_{sd,i} d_i C_i}{1 + d_i C_i}, \ \forall i \in Components, \ \forall z \in (0, L) \quad (5)$$

$$b_i = b_0 e^{(-\Delta H_{b,i}/RT)} \quad (6)$$

$$d_i = d_0 e^{(-\Delta H_{d,i}/RT)} \quad (7)$$

where $q_{sb,i}$ is the maximum equilibrium adsorption amount of species i on site 1 [mol/kg$_{ads}$], $q_{sd,i}$ is the maximum equilibrium adsorption amount of species i on site 2 [mol/kg$_{ads}$], b_i and d_i are equilibrium absorption constants [m^3/kmol], b_o and d_0 are pre-exponential constants [K], $\Delta H_{b,i}$ and $\Delta H_{d,i}$ are the heat of adsorptions at each site [J/mol], R is the universal gas constant [J/mol/K], and T is the temperature [K]. The equilibrium parameters b_i and d_i, in equations (6) and (7) respectively, follow the Van't Hoff equilibrium temperature dependence equation [72]. The momentum balance/pressure drop along each column is expressed through the Ergun equation [78]:

$$-\frac{\partial P}{\partial z} = 150 \frac{\mu_g (1-\varepsilon)^2}{\varepsilon^3 d_p^2} v_s + 1.75 \frac{(1-\varepsilon)}{\varepsilon^3 d_p} \rho_g {v_s}^2, \ \forall z \in (0, L) \quad (8)$$

where P is the pressure [bar], μ_g is the dynamic viscosity [Pa.s], d_p is the pellet particle diameter [m] and ρ_g is the fluid phase mass density [kg/m^3]. The model is non-isothermal and non-adiabatic, accounting for heat transfer between the bed and column wall using thermal inertia properties of the column (i.e. thermal conductivity and specific heat capacity), excluding heat transfer between the solid adsorbent and gas flow, i.e. thermal equilibrium. The fluid phase energy balance [79]:

$$\frac{\partial U_{bed}}{\partial t} = \varepsilon \frac{\partial}{\partial z} \left(\rho_T D_L \frac{\partial H_f}{\partial z} \right) - \frac{\partial \left(v_s \rho_T H_f \right)}{\partial z} + \frac{1}{1000} \frac{\partial}{\partial z} \left(\lambda_e \frac{\partial T}{\partial z} \right) + - \frac{4 h_W}{d_b} \frac{1}{1000} \left(T_f - T_w \right), \ \forall z \in (0, L) \quad (9)$$

where U_{bed} is the energy per unit volume of the bed [kJ/m^3], H_f is the bulk fluid phase mass specific enthalpy [kJ/kg], ρ_T is the total mass density of the fluid phase [kg/m^3], λ_e is the effective axial thermal conductivity [W/m^2/K], h_W heat transfer coefficient between the gas and column wall [W/m^2/K], d_b is the bed diameter [m], T_f is the fluid phase temperature [K] and T_w is the bed wall temperature [K]. Assuming axial flow is from the feed to the product side of the adsorption column, the boundary conditions are:

$$\frac{F^{in} H_f^{in}}{A_{bed}} = v_s \rho_T H_f - \varepsilon D_L \rho_T \frac{\partial H_f}{\partial z} - \frac{1}{1000} \lambda_e \frac{\partial T}{\partial z}, \ \forall z \in (0, L) \quad (10)$$

$$\frac{\partial T}{\partial z} = 0, \ z = L \quad (11)$$

where F^{in} is the mass flowrate entering the bed [kg/s], and H_f^{in} is the mass specific enthalpy of the entering fluid on the feed side of the adsorption bed [kJ/kg]. Taking into consideration the thermal inertia and conduction within the bed wall, the energy balance for the metal wall is [79]:

$$\rho_w C_{p,w} A_w \frac{\partial T_w}{\partial t} = A_w \lambda_w \frac{\partial^2 T_w}{\partial z^2} + h_w \frac{4}{d_b} \left(T_f - T_w \right) + h_{w,a} \frac{4(d_b + 2 l_w)}{d_b^2} (T_w - T_a), \ \forall z \in (0, L) \quad (12)$$

where ρ_w is the bed wall mass density [kg/m^3], $C_{p,w}$ is the bed wall specific heat capacity [kJ/kg/K], A_w is the bed wall cross-sectional area [m^2], T_a is the ambient temperature [K], λ_w is the wall material thermal conductivity [W/m/K], $h_{w,a}$ heat transfer coefficient between the column wall and external environment [W/m^2/K] and l_w is the wall thickness [m].

Process simulation tools such as Aspen Adsorption [57,58,64,80] and gPROMS ProcessBuilder [81,82], have been used to effectively simulate, analyse and optimise CO_2/N_2 adsorption. In this study, the model is developed in gPROMS ProcessBuilder utilising the physical properties package Multiflash™. Adsorption processes are inherently dynamic; therefore, the process models must include valves to control the flow in and out of the adsorption bed. For this study each valve is considered adiabatic, where the mass flowrate (F in kg/s) and pressure drop (Δp) are related through:

$$F = C_v x \Delta p \quad (13)$$

As the model is pressure driven, the flow coefficient (C_v in kg/s/kPa) for each valve is calculated to give the required pressure drop during each stage of the simulation. The timings of the valve stem position (x) are defined using a scheduling unit. This controls which valves are open at any given time, allowing for step management and cyclic behaviour.

The energy demand comes from the compressors needed to elevate the bed pressure and the vacuum pumps needed to depressurise the bed to desorb the CO_2. For real gas compression and evacuation power consumption [W], Nikolaidis et al. [32] used:

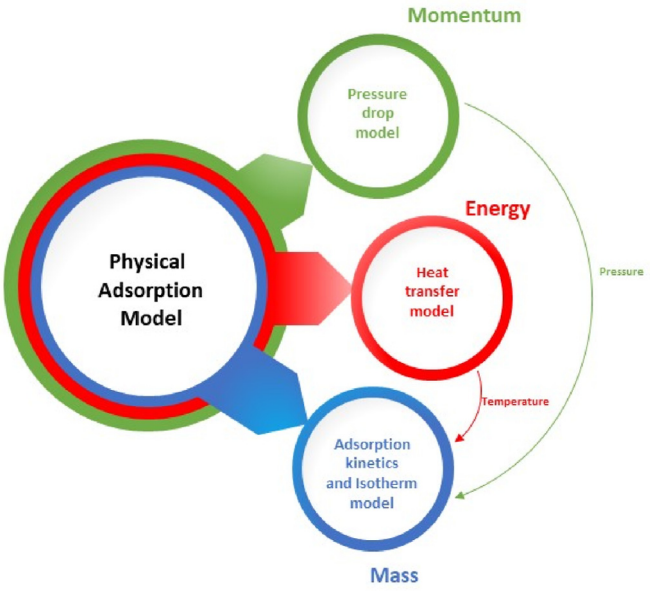

Fig. 2. Physical adsorption model components.

$$Power_{comp} = F_{in} T_{in} R \frac{1}{n_c} \left(\frac{\gamma}{\gamma - 1}\right) \left[\left(\frac{P_{out}}{P_{atm}}\right)^{\frac{\gamma-1}{\gamma}} - 1\right] \quad 14$$

$$Power_{vac} = F_{in} T_{in} R \frac{1}{n_v} \left(\frac{\gamma}{\gamma - 1}\right) \left[\left(\frac{P_{atm}}{P_{vac}}\right)^{\frac{\gamma-1}{\gamma}} - 1\right] \quad 15$$

where F_{in} is the inlet flowrate [mol/s)], T_{in} is the inlet temperature [K], R is the universal gas constant [J/mol/K], P_{out} is the compressors discharge pressure [Pa], P_{atm} is atmospheric pressure [Pa], and P_{vac} is the vacuum pressure draw [Pa]. The ratio of specific heat capacities (γ), also known as the adiabatic constant, is assumed to be 1.4. Within the literature the isentropic efficiency (n_c and n_v) for N_2/CO_2 systems is 0.72 [54]. To compare and evaluate CCA technologies two important metrics are used: recovery rate (difference between the mass of CO_2 entering and exiting the process) and the purity (end CO_2 composition). Alongside these metrics are two important performance indicators: the specific energy demand (E_T) calculated using equation (16) and the Productivity (P_r) calculated using equation (17).

$$E_T[kWh / tCO_2] = \frac{TotalEnergyDemand[kWh]}{MassofCO_2Captured[ton]} \quad 16$$

$$P_r\left[mol \,/\, m^3 Adsorbent \,/\, s\right] = \frac{CO_2Captured[mol]}{VolumeofAdsorbent\left[m^3\right] \times totalcycletime[s]} \quad 17$$

2.2. Single column validation

In order to evaluate the validity of the process model, a single column is validated against pilot scale data from Krishnamurthy et al. [38]. The pilot study investigated CO_2/N_2 VPSA on the commercial sorbent Zeolite 13X. The feed contains 15 mol.% CO_2 and 85 mol.% N_2 at 1000 SLPM. The column specifications are shown in Table 3.

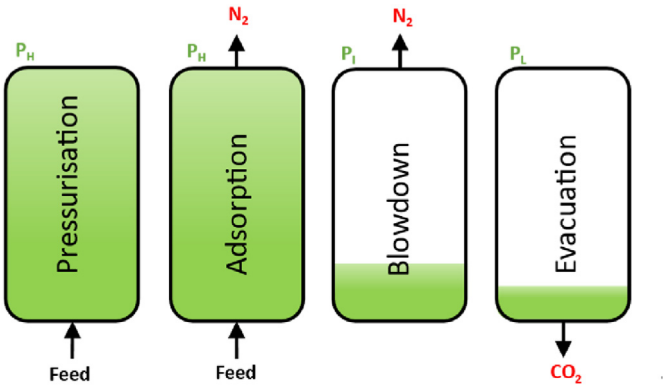

Fig. 3. Four-step VPSA cycle.

Run 1 in Ref. [38] is chosen for its high CO_2 purity (94.7 ± 1.05%) and high CO_2 recovery (85.4 ± 4.52%). The four-step Skarstrom cycle VPSA system includes: (i) pressurisation to P_H using the feed gas, (ii) adsorption at high pressure with product valve open, (iii) forward blowdown to depressurise the column to P_i, and (iv) reverse evacuation to recover CO_2 at P_L (see Fig. 3). The step duration and pressure specifications are shown in Table 4.\

The gravimetric equilibrium isotherm data is shown in Table 5. Zeolite 13X is a Faujisite type zeolite, and [83] determined the thermal conductivity to be 2.28 (W/m/K). Mass transfer coefficients for N_2 and CO_2 on Zeolite 13X are taken as 2.733 s^{-1} and 0.065 s^{-1} respectively, and the axially dispersion co-efficient is 0.23 m^2/s [48]. Table 6 highlights the other key process parameters necessary to calculate the mass and heat transfer along the adsorption column.

Fig. 4 compares the simulations adsorption bed pressure and temperature against the pilot results (Run 1) from Krishnamurthy et al. [38]. The simulation exhibits an almost identical pressure increase during the pressurisation step (t = 0–20s), using 1000 SLPM flowrate containing 85 mol.% N_2 and 15 mol.% CO_2. During the adsorption (t = 20–80s) and blowdown (t = 80–230s) steps, similar pressure profiles are seen between the simulation and pilot results, the pressure drop rate is slightly greater in the pilot test, however, both results produce a bed pressure of 0.07 bar once the blowdown step is complete. Small variations between the results could be due to data extraction errors, as the pilot experiments performance indicators are for the 300th cycle; however, individual error bars are not available for the dynamic pilot results. Included in Fig. 4 is the feed and product header temperatures, within Krishnamurthy et al. [38] the temperature profile is not given for a single cycle; however, they have been included to compare with the full-scale VPSA simulations.

Two important key performance indicators for CO_2 capture

technologies are the recovery rate and CO_2 purity. The recovery rate is defined as the percentage difference between the CO_2 flow entering and exiting the system [5]; in this case, the flowrates (Fig. 5) and compositions (Fig. 6) are used to calculate the amount of CO_2 captured (84.30%), which lies within the bounds (85.4 ± 4.52%) specified in Krishnamurthy et al. [38]. The purity of the end product during the evacuation step in the simulation is 89.56% (mol/mol), 5.14% points lower than the pilot facility (94.7 ± 1.05%). The simulation's predicted purity is not only a function of bed dynamics, in particular the adsorption rate calculated through the isotherm model, it is also affected by the valve stem position and the flowrate through the evacuation valve. As multiple factors affect the purity it is difficult to align all the input parameters simultaneously in order to improve the results. Also, as the model is pressure driven it is vital the pressure profile is as accurate as possible. Therefore, the evacuation valve and flowrate cannot be further adjusted (to increase the purity), as this would prevent the pressure level from decreasing to the 0.025 bar goal.

Fig. 5 compares the flowrates exiting the adsorption column, and the composition profiles during the adsorption, blowdown and evacuation steps are shown in Fig. 6. The adsorption flowrate exiting the top of the column (mainly composed of N_2) exhibits a similar profile to the bed pressure. The pilot evacuation profile shows a smaller decease in flowrate compared to the simulation, due to a rapid pressure drop from the intermediate pressure (0.07 bar) to the low pressure (0.025 bar) used to desorb the captured CO_2.

The pilot results productivity was 1.4 tCO_2/m^3/day, the simulation result is 15% lower at 1.18 tCO_2/m^3/day. The overall power demand (for the flue gas blower and vacuum pumps) is 934.05 kWh/tCO_2, 74.26% higher than the pilot run power demand (510.5 ± 25.5 kWh/tCO_2). If the efficiency of the pumps is set at 100% the overall power demand is 672.52 kWh/tCO_2 and 25.47% higher than the pilot test. The accuracy is further improved if the ratio of specific heat capacities is closer to that of CO_2 (1.28 [84]), specifically during the evacuation step due to the higher CO_2

Table 3
Single column specifications [38].

Parameter	Value
Column internal diameter (m)	0.3
Column packing height (m)	0.867
Mass of adsorbent (kg)	41
Particle size (mm)	1.6–2.6
Bed Voidage	0.428

Table 4
Step duration and pressure specifications [38].

Step	Time (s)	Pressure (level)	Pressure (bar)
Pressurisation	20	P_H	1.5
Adsorption	60	P_H	1.5
Blowdown	150	P_i	0.07
Evacuation	310	P_L	0.025

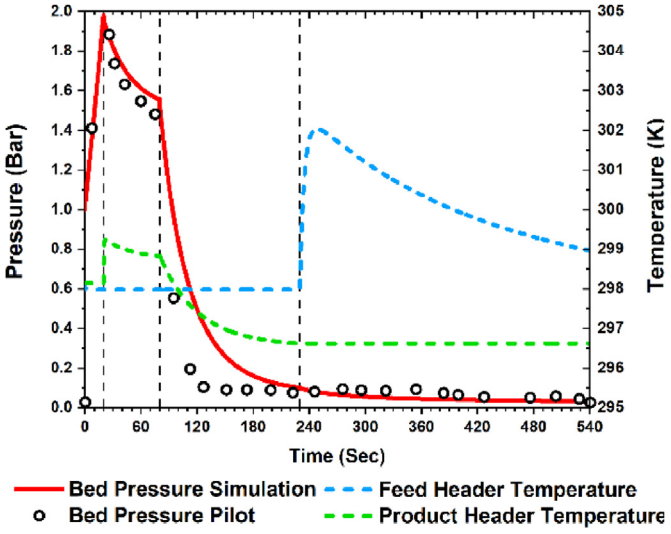

Fig. 4. Adsorption bed pressure and temperature profiles.

Table 5
Dual-site Langmuir isotherm parameters [76].

Parameter	Symbol	N_2	CO_2
Equilibrium adsorption amount for site 1 (mol/kg)	$q_{sb,i}$	5.84	3.09
Equilibrium adsorption amount for site 2 (mol/kg)	$q_{sd,i}$	0	2.54
Pre-exponential constant for site 1 (m^3/mol)	b_0	2.50x10-6	8.65x10-7
Pre-exponential constant for site 2 (m^3/mol)	d_0	0	2.63x10-8
Heat of adsorption for site 1 (J/mol)	$-\Delta H_{b,i}$	−1580000	−36641.21
Heat of adsorption for site 2 (J/mol)	$-\Delta H_{d,i}$	0	−35690.66

Table 6
Mass and heat transfer parameters [76].

Parameter	Symbol	Value
Pellet bulk density (kg/m^3)	–	1130
Pellet void fraction (m^3/m^3)	–	0.35
Specific heat capacity of fluid (J/mol/K)	–	30.7
Specific heat capacity of adsorbent (J/kg/K)	–	1070
Wall thickness (mm)	l_w	17.5
Wall density (kg/m^3)	ρ_w	7800
Heat transfer coefficient between bed and wall (W/m^2/K)	h_w	8.6
Heat transfer coefficient between wall and environment (W/m^2/K)	$h_{w,a}$	2.5
Specific heat capacity of the column wall (J/kg/K)	$C_{p,w}$	502
Thermal conductivity of the column wall (W/m/K)	λ_w	16
Universal gas constant (m^3 Pa/mol/K)	R	8.314

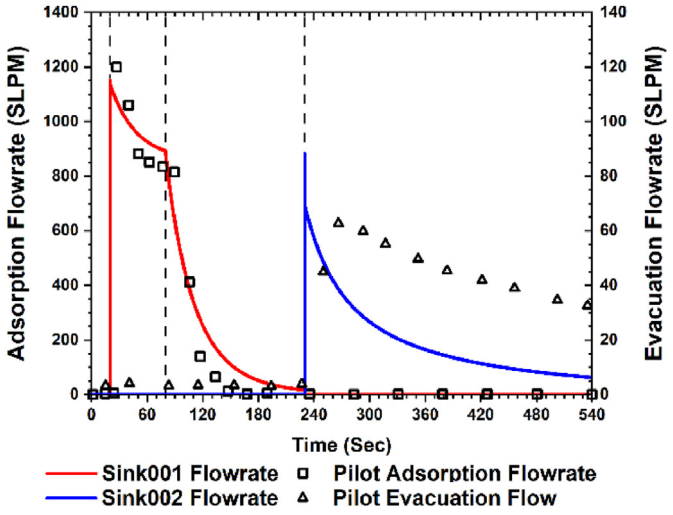

Fig. 5. Flowrate profiles for the adsorption/blowdown and evacuation steps.

concentration, the power demand is 611.79 kWh/tCO_2 and 14.14% higher than the upper bound of the pilot test. Highlighting the need for variable specific heat capacity ratios when determining overall pump power requirement.

During the adsorption step the average adsorption amount for CO_2 and N_2 is 3.569 mmol/g and 0.464 mmol/g, respectively, comparable to sources in the literature looking specifically at Zeolite 13X [85,86]. Even though the CO_2 concentration leaving the column is lower than expected, the accuracy of the capture rate and the adsorption capacity shows the fidelity of the overall process model.

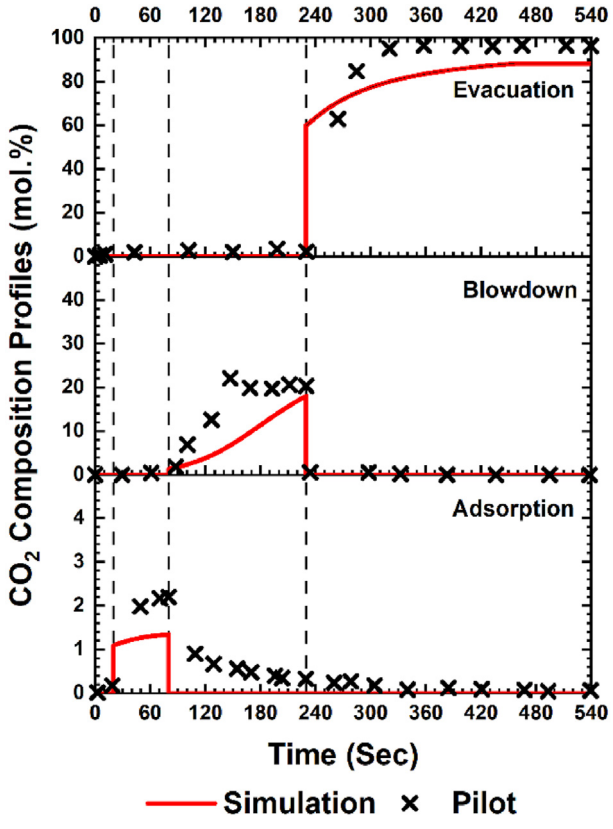

Fig. 6. Comparison of CO_2 composition profiles during the Adsorption, Blowdown and Evacuation steps.

3. Large-scale system design

Large-scale CCA systems require multiple beds and multiple stages for continuous separation of the desired component. A limitation for large-scale vacuum-adsorption systems is the ability of industrial machinery to deliver the vacuum pressure necessary for desorption [87], i.e., the vacuum pressures achieved in lab/pilot-scale systems may not be achievable at large-scale [33]. Therefore, the large-scale VPSA system used in this study is based on Luberti et al. [33], where the 1st stage is split into two identical two-bed VPSA units to handle the large inlet flowrate. The process topology for this studies adsorption CO_2 capture system is shown in Fig. 7. In Shen et al. [30], Wang et al. [17], and Luberti et al. [33] a secondary stage in series is used to ensure the end CO_2 purity is above 95%; however, in this study the purity is already >95% meaning the second stage is not required. In Fig. 7, the scheduling unit dictates the valve stem position (x in Equation (13)), i.e., how open the valve is. The valve flow coefficient (C_V in Equation (13)) is specified to give an adequate pressure drop over each valve.

Assuming the power generation source is a 10 MWe open-cycle gas turbine (OCGT), 33.8 kg/s of flue gas is produced with 4.27 vol% CO_2 (6.78 wt% or 4.42 mol.%) [7]. Each parallel train processes 16.9 kg/s of flue gas (FGS1 and FGS2 on Fig. 7). The process simulation uses the same isotherm (Table 5) and mass and heat transfer parameters (Table 6) as the validation study. In order to process the large flue gas flowrate, the column properties are scaled such that each adsorption column has 11.15 m packing height, 4.80 m bed diameter, 2 mm particle size, and the bed voidage is 0.428. These column properties ensured the scaled design has the same adsorbent surface area to volume ratio (3000 m^2/m^3) as the pilot study.

The scheduling unit dictates the valve stem positions, within Fig. 7 the scheduling table highlights each valves stem position during each of the two bed four step operations, i.e., Press − Bb denotes the first bed is in pressurisation mode and the second bed is in blowdown mode.

Also included in Fig. 7 is the scheduling table that highlights each valve's flow co-efficient used in Equation (13) to calculate each valve's pressure drop. Similarly to the pilot study used for the validation simulation, the scaled-up system design has four process steps with three main target pressures. The step timings and corresponding pressure levels are shown in Table 7. The Finite Volume Method is selected as the numerical discretisation scheme. There are 10 discretisation points per layer (one layer in total) with uniform distribution across the layer. The structural analysis for the Baseline process model showed the total number of model equations is 2,781, with 3191 process variables (2, 781 unknown and 410 inputs) and 18,327 parameters. The 5-h operation was simulated in 879 s (CPU).

3.1. Flexible operation

The flexible operation of OCGT's is based on our previous work [7], which analysed data from the Balancing Mechanism Report Services (BMRS) and industrial gas turbine suppliers, to show the typical operation of OCGT's in the UK. The results showed the highly transient nature of OCGT power generation, with average operating times around 5 h, while ramping to different power outputs within the same operating window. Fig. 8 is an example OCGT operation for a 10 MWe plant, using a Siemens SGT-400 gas turbine. The OCGT can ramp to different power outputs at a rate of 10% baseload (MWe) per minute, and the start-up and shutdown rates are 12.5% baseload (MWe) per minute [88]. Therefore, the

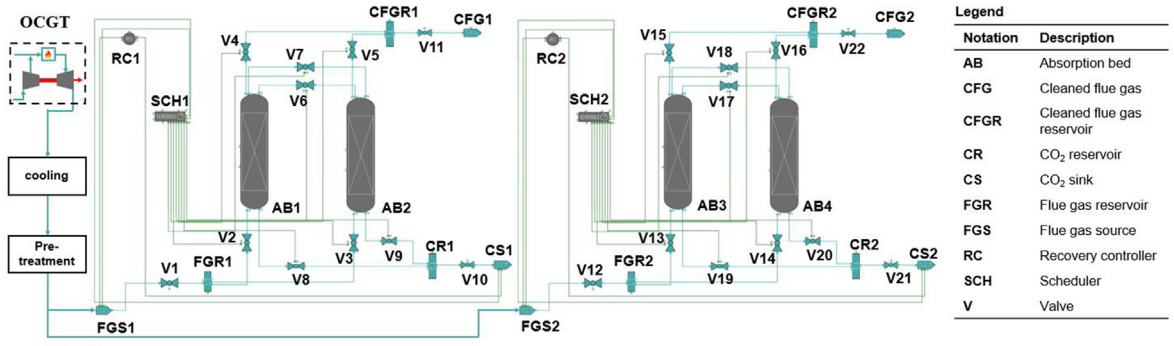

Schedule

Steps	V1	V2	V3	V4	V5	V6	V7	V8	V9	V10	V11	V12	V13	V14	V15	V16	V17	V18	V19	V20	V21	V22
Press – Bd	1	1	0	0	1	0	0	0	0	1	1	1	1	0	0	1	0	0	0	0	1	1
Ads – Ev	1	1	0	1	0	0.1	0	0	1	1	1	1	1	0	1	0	0.1	0	0	1	1	1
Bd – Press	1	0	1	1	0	0	0	0	0	1	1	1	0	1	1	0	0	0	0	0	1	1
Ev – Ads	1	0	1	0	1	0	0.1	1	0	1	1	1	0	1	0	1	0	0.1	1	0	1	1
C_V (kg/s/kPa)	20	88	88	84.4	84.4	0.15	0.15	8.2	8.2	0.34	8	20	88	88	84.4	84.4	0.15	0.15	8.2	8.2	0.34	8

Press = Pressurisation, Ads = Adsorption, Bd = Blowdown, and Ev = Evacuation

Fig. 7. Large-scale VPSA model topology, where the flue gas stream is split into two parallel streams, included in the figure is valve scheduling and each valve's flow co-efficient.

Table 7
Step duration and pressure specification for the large-scale VPSA system.

Step	Time (s)	Pressure (level)	Pressure (bar)
Pressurisation	80	P_H	1.5
Adsorption	220	P_H	1.5
Blowdown	80	P_i	0.07
Evacuation	220	P_L	0.025

start-up/shutdown time is 8 min, the ramp time to 70% load is 3 min, and the ramp time to 50% load is 5 min. The balancing period in the UK is 30 min [89]. Each new load is maintained until the end of the 2nd balancing period before ramping or shutdown is performed, i.e., at 60 min the flue gas is ramped to 70% load in 3 min, 57 min later the flue gas is then ramped back up to full load. As the total cycle operating time is 600 s, 31 cycles are required for a 5-h operation plus the 8-min shutdown time.

4. Results

The results section shows the large-scale VPSA operation, during the Baseline (no transient behaviour) and Flexible (transient flue gas input) operating scenarios. The scaled system analysis focusses on the effects transient operation has on the processes key performance indicators (KPI), this study does not look at the optimisation of the scaled VPSA design. Fig. 9 shows the flowrates through flue gas source (FGS), cleaned flue gas (CFG) and CO_2 sink (CS) streams, these are highlighted in Fig. 7, for both the Baseline and Flexible operating scenario. Each parallel train handles 16.9 kg/s exhaust flow. The flowrate profiles for the CFG and CS flows are similar to the pilot study, where there is a sharp initial spike in flow that levels out during each operating step. When one bed is adsorbing the other bed is evacuating, allowing for continuous CO_2 capture. In the Baseline scenario, the system is fed with a constant flue gas flowrate for the entire 5-h operating period. In the Flexible scenario, the system is fed with a transient flue gas supply. Included in this scenario is the start-up procedure, ramping to 70% and 50% loads, and the shutdown procedure. Due to computational limitations the simulation cannot operate at 0 kg/s feed, therefore, the system starts at 0.9 kg/s and ramps to 16.9 kg/s during start-up in 8 min. Similarly, for the shutdown operation, the feed is at 16.9 kg/s and ramps to 0.9 kg/s in 8 min.

Fig. 10 presents the adsorption bed (AB1 and AB2 on Fig. 7) pressure profiles during the Baseline and Flexible operating

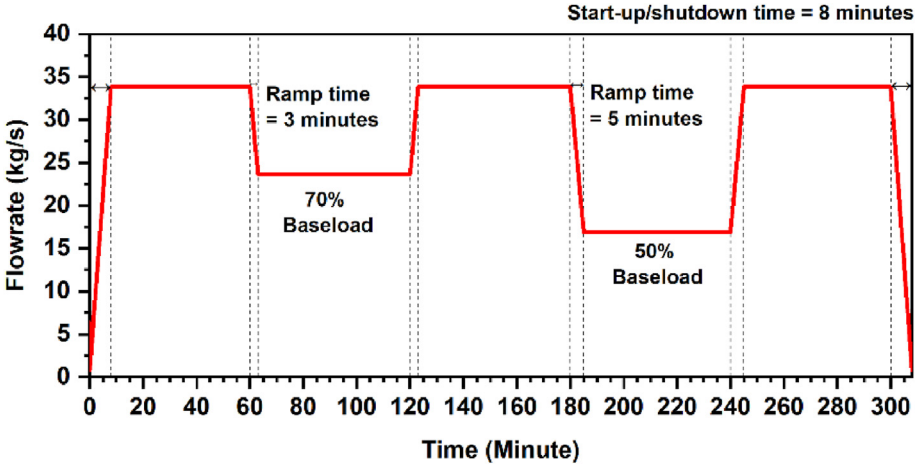

Fig. 8. Transient OCGT operation from Wilkes et al. [7].

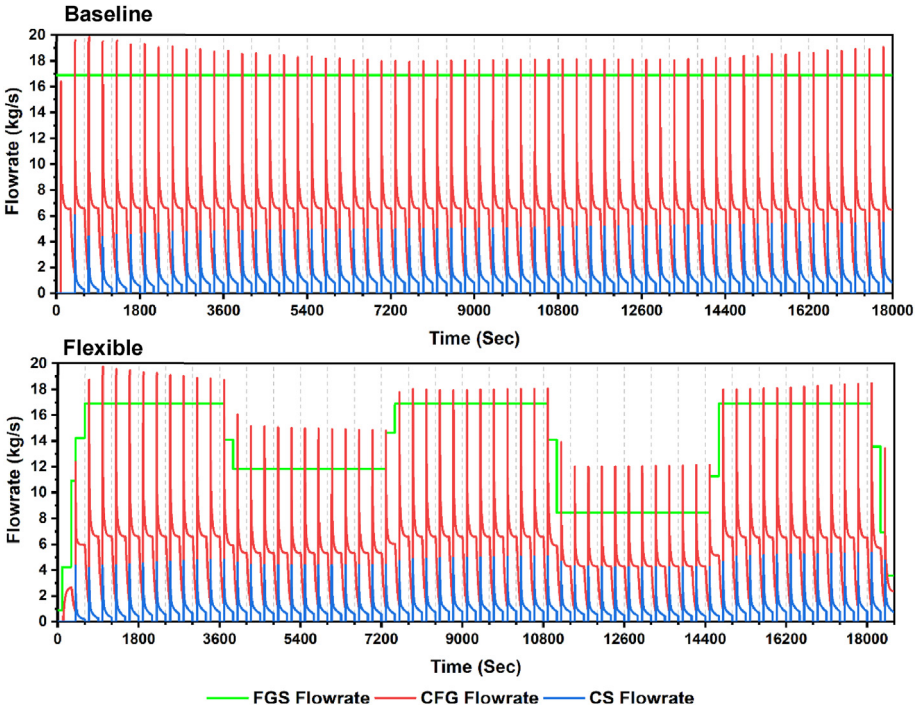

Fig. 9. Flowrate profiles for the flue gas source (FGS), cleaned flue gas (CFG) and CO_2 sink (CS) flowrates in each of the parallel VPSA units, during the Baseline and Flexible scenarios.

scenarios. The profiles are comparable to the pilot-scale study, see Fig. 4. As the models are pressure driven it is important the pressure profiles are accurate. There is a sharp initial increase in pressure (pressurisation step), which then equalises during the adsorption step when the product valves are opened. At t = 300 s in each adsorption cycle the blowdown valves (V4, V5, V15, and V16 in Fig. 7) are opened and the bed pressure drops to 0.07 bar, at t = 500 s in each cycle the blowdown valve is closed, and the evacuation valve is opened (V8, V9, V19, and V20 in Fig. 7), further reducing the bed pressure to 0.025 bar and the CO_2 is desorbed from the bed. In the Flexible scenario the valve coefficient for V6, V7, V17, and V18 is changed from 0.15 to 0.01 kg/s/kPa to ensure an adequate exchange between the adsorption columns during the low load (50%) operation, without this alteration the full operation could not be completed.

Over the course of operation there is a gradual increase in the initial pressure spike during the pressurisation step. During the pressurisation step in the first cycle (Baseline operation), the bed pressure (AB1) is elevated to 1.47 bar. Whereas, in the final cycle the bed pressure is elevated to 1.76 bar. This is a result of the increasing column temperature, especially at the bottom of column, shown in Fig. 11. The increase in step pressure is also shown in the pilot scale results in Krishnamurthy et al. [38]. At the end of each adsorption cycle the columns equalise to 0.025 bar ready for the next adsorption cycle.

During the Flexible scenario, less flow is going through the system during the start-up, ramping and shutdown periods, therefore the adsorption columns cannot pressurise to 1.5 bar. Hence, the bed pressure follows the same profile as the input (FGS) flowrate. The valve flow coefficients are set input parameters that are used alongside the flowrate to calculate the pressure drop across the valve. Incorporating control systems to modify the flow coefficients during low load operation could promote acceptable pressure increases in the column. However, this would involve developing Model Predictive Control (MPC) strategies, which is beyond the scope of this study. Several studies have investigated optimisation and control strategies for Flexible-MEA systems [90,91] and flexible gas turbines [92], which have provided valuable information on the potential options available to reduce the specific energy of the processes. Therefore, future work should focus on optimising and developing strategies specifically for Flexible-VPSA systems.

The temperature profile in the adsorption column changes throughout each of the 5-h operations, Figs. 11 and 12 show this transient behaviour for the Baseline and Flexible scenarios, respectively. As the adsorption process releases the heat of adsorption when CO_2 is adsorbed, the temperature increases in the column. In the beginning of the operation, the temperature bulge is located at the bottom of the column; indicating most of the adsorption is taking place within the first 2 m of packing. The temperature bulge transitions towards the centre of the column (between 4 and 8 m) as the operation progresses.

There is a small difference in the rate at which the temperature increases in the first operating cycle, between the Baseline and Flexible operating scenarios. This is due to the start-up procedure lasting 480 s; therefore, it is at full-load by the end of the first operating cycle. As less CO_2 is entering the system, less CO_2 is adsorbed onto the zeolite surface and less heat is emitted into the column. There is also a sudden drop in temperature in the Flexible scenario in the bottom of the column between t = 10000 to t = 14000 s, due to decreasing the inlet flowrate to 50% load. Overall, there is a small difference in the temperature increase (<1.5K) at the temperature bulge, highlighting that less CO_2 is being adsorbed in the column.

The dissimilarities between scaled Baseline and pilot KPI results (see Table 8) are related to the scaled system design. The adsorption

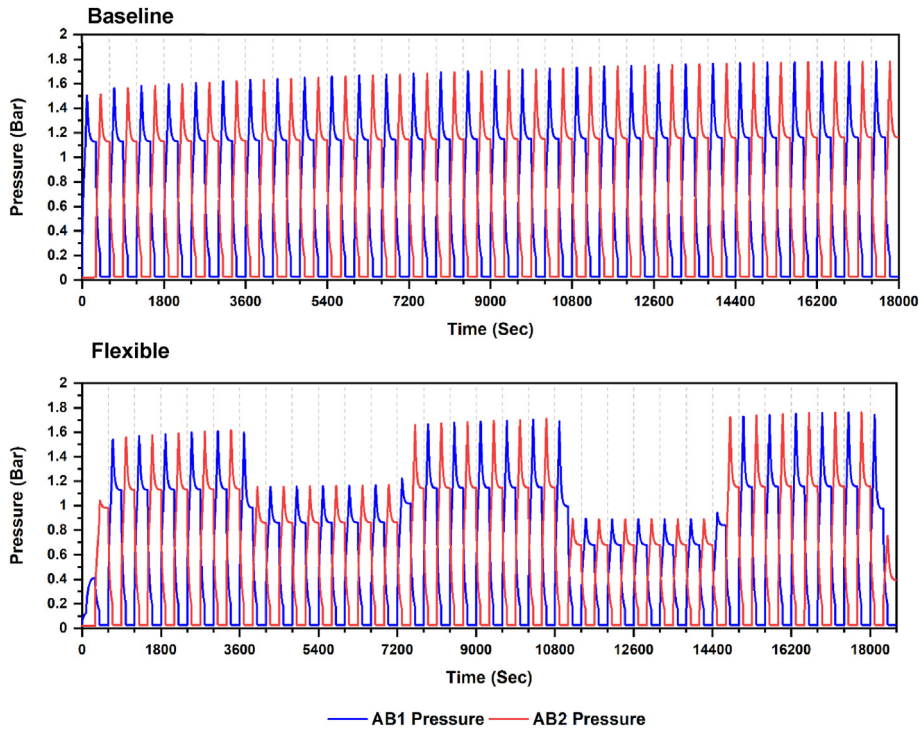

Fig. 10. Pressure profiles for adsorption bed 1 (AB1) and adsorption bed 2 (AB2) in each of the parallel VPSA units, during the Baseline and Flexible scenarios.

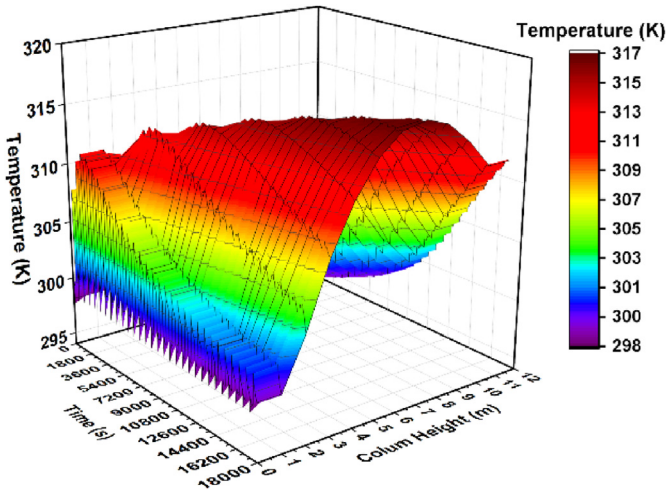

Fig. 11. Adsorption bed (AB1) 3-D temperature profile for the Baseline scenario.

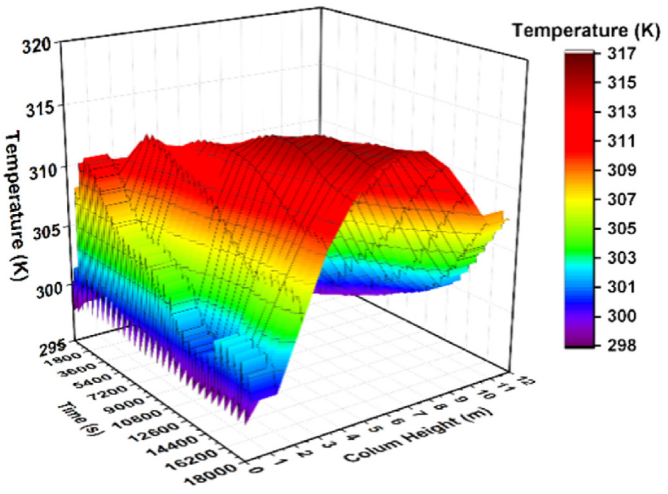

Fig. 12. Adsorption bed (AB1) 3-D temperature profile for the Flexible scenario.

cycle steps and timings were modified for continuous operation. The timings used in this study enabled the large adsorption columns to pressurise and minimise the inlet FGS velocity, preventing issues such as flow reversal, increased pressure drop, and loss in separation efficiency. Krishnamurthy et al. [38] showed the effect of altering the step duration and blowdown pressure on the recovery rate and purity. Longer adsorption step times increases the purity and decreases the recovery rate, due to the CO_2 front moving further into the column. This is observed in the 3-D temperature profile, see Fig. 11. Highlighting, the adsorption timing within this study needs to be longer, however, this is limited by the pressure increase in the bed. Parameter scaling is another important issue: without demonstration scale results it is difficult to ascertain the fidelity of the scaled models [93].

The continuous operation and modified step timings also explain the increase in energy demand. The scaled Baseline results are more than double the pilot scale results, due to constant flue gas processing (increased flow through the FGS blower, CFG vacuum pump, and CS vacuum pump), thus requiring more energy. Despite the issues with the scaled design, it is important to see the ramifications transient operation has on the performance of VPSA CO_2 capture.

An issue observed in industrial adsorption processes is complex valve operation [94,95]. Within this study the valves are operated based on flow co-efficients dictating the pressure drop. Each valve operates simultaneously with the active status constantly changing. The complex partnership between the valves within the system make scaling up the VPSA processes difficult and affects the KPI's.

Table 8
Key performance indicators (KPI) for the Baseline and Flexible VPSA simulations.

KPI	Pilot [38]	Scaled-Baseline	Deviation (%)	Scaled- Flexible	Deviation (%)
Recovery rate (%)	85.40 ± 4.52	97.07	+13.66	97.03	−0.04
Purity (%)	94.7 ± 1.05	80.74	−14.74	79.54	−1.49
Energy demand (kWh/tCO_2)	510.5 ± 25.5	1191.72	+133.67	1274.04	+6.91
Productivity (tCO_2/m^3 ads/day)	1.40 ± 0.07	1.28	−9.02	1.07	−15.85

When scaling the VPSA design it is important to consider the adsorption steps and timings, column geometry, process design and valve operation.

The differences between the Baseline and Flexible operating scenarios KPI's can be explained by the non-identical temperature profiles in Figs. 11 and 12. In this study, for VPSA there is a small drop in recovery rate (0.03% points). This is lower than all of the MEA CO_2 capture flexible response scenarios (0.73−1.20% points lower than the steady-state results at 92.48%) shown in Wilkes et al. [7]. There is also a small drop in purity for flexible VPSA system (1.20% points). Although Wilkes et al. [7] do not specify the end purity, their report states there is also a drop in purity during flexible operation. This will affect downstream compression equipment, so too will the transient operation [96].

Fig. 13 highlights the FGS blower, CFG vacuum pump and CS vacuum pump power requirements for the Baseline and Flexible scenarios. The majority of the energy demand comes from the CFG vacuum pump used in the adsorption and reverse blowdown steps. This has the largest energy demand because it handles a large amount of flow compared to the CS vacuum pump, and the energy drop is the greatest (approximately 1.5 to 0.07 bar). Despite the Flexible scenario consuming less energy, it has a higher specific energy demand (see Table 8) due to the smaller quantity of CO_2 captured (see Fig. 13). The quantity of CO_2 captured during the Baseline (39.99 tCO_2/operation) and Flexible (33.65 tCO_2/operation) operations are comparable to the results in Wilkes et al. [7] (31−37 tCO_2/operation), the slightly higher amount is due to the higher capture rate (92.48% MEA steady-state results).

Several studies have highlighted the use of MPC strategies for solvent-based [97] and adsorption [90,98] capture technologies. It has been observed that MPC can improve the capture performance and aid in reducing deviations caused by flexible operation [99,100]. Neither the VPSA system analysed in this study, nor the MEA system analysed in Wilkes et al. [7] include MPC, as these studies focus on the technical feasibility of transient operation. Future work should incorporate MPC strategies to optimise the performance of dispatchable OCGT-PCC, specifically at low-load operation.

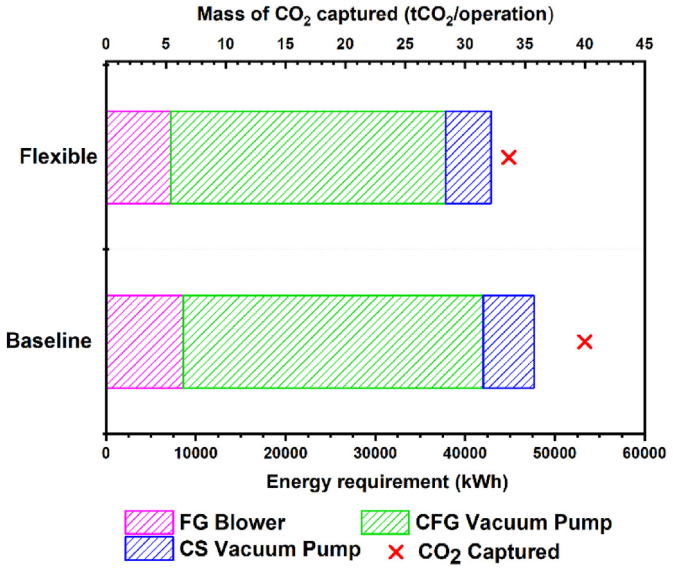

Fig. 13. Pump energy requirement and mass of CO_2 captured during the 5-h operation for the Baseline and Flexible scenarios.

5. Conclusion

As the need for flexible CO_2 captured increases, alternate technologies to amine-based post-combustion capture (PCC) need to be investigated specially for flexible response. Within this study a vacuum-pressure swing adsorption (VPSA) PCC system has been modelled, validated, and scaled up to process flow from a small-scale 10 MWe open-cycle gas turbine (OCGT). The purpose of the study is to assess the ability of a VPSA CO_2 Capture system to handle highly transient flue gas operation, to highlight the technologies applicability in future energy systems that require fast-response dispatchable generators to combat intermittent renewables. The validation study showed the process model accurately simulated the adsorption of CO_2 on the Zeolite 13X sorbent. The amount of CO_2 captured (84.30%) lies within the error bounds (85.4 ± 4.52%) specified in that pilot-scale study [38].

The full-scale simulations showed the limitations with process scaling for VPSA systems are related to adsorption step timings, column sizing, and valve operation. The aim of the paper is not to provide scaled system design, but to investigate the effects of flexible operation on VPSA CO_2 capture. To the authors knowledge, no studies have investigated Flexible-VPSA, i.e., the effects of transient flue gas production on the operation and performance of VPSA CO_2 capture. Included in the Flexible-VPSA operation is the start-up, ramping, and shutdown procedures. The simulations showed minimal deviation in CO_2 purity (−1.49%) and recovery rate (−0.04%), between the Baseline and Flexible operating scenarios. The decrease in purity and recovery rate during flexible operation is lower than experienced in MEA based Flexible-PCC.

As demonstrated in our earlier study, the energy demand for MEA based Flexible-PCC varies between each of the flexible operating scenarios investigated [7]. When the steam supply to the reboiler (for solvent regeneration) is constant, the energy demand for the process is 4.69 GJ/tCO_2 (1302.78 kWh/tCO_2). When the steam supply is altered in accordance with flue gas changes, the energy demand decreases to 3.95 GJ/tCO_2 (1097.22 kWh/tCO_2). For Flexible-VPSA the energy demand (for the blower and vacuum pumps) is 4.59 GJ/tCO_2 and 16.11% higher than the best Flexible-MEA case. This is due to the fact that no specific energy minimisation scenario was considered in this study. Therefore, future work should focus on developing dedicated operating scenarios and control strategies for a VPSA system, in order to minimise the negative energy effects of transient operation and scale-up. A possible solution is manipulating the scheduling (step time and pressure level) to deliver lower specific energy demands for the pumps during low load operation.

Credit author statement

Mathew Wilkes: Conceptualization, Methodology, Investigation Software. Solomon Brown: Supervision, Writing- Reviewing and Editing.

Declaration of competing interest

The authors declare that they have no known competing financial interests or personal relationships that could have appeared to influence the work reported in this paper.

Acknowledgements

This work is funded by the Engineering and Physical Sciences Research Council (EPSRC) Centre for Doctoral Training in Carbon Capture and Storage and Cleaner Fossil Energy (reference: EP/L016362/1), and Drax Group Plc. The second author would like to acknowledge support of the Royal Academy of Engineering through the Industrial Fellowship (reference: IF\192046).

References

[1] Heuberger CF, Mac Dowell N. Real-world challenges with a rapid transition to 100% renewable power system. Joule 2018;2(3):367–70.
[2] Mac Dowell N, Staffell I. The role of flexible CCS in the UK's future energy system. Int J Greenh Gas Control 2016;48(2):327–44.
[3] Huber M, Dimkova D, Hamacher T. Integration of wind and solar power in Europe: assessment of flexibility requirements. Energy 2014;69:236–46.
[4] Mac Dowell N, Shah N. Optimisation of post-combustion CO2 capture for flexible operation. Energy Proc 2014;63:1525–35.
[5] Bui M, Tait P, Lucquiaud M, Mac Dowell N. Dynamic operation and modelling of amine-based CO2 capture at pilot scale. Int J Greenh Gas Control 2018;79:134–53.
[6] Tait P, Buschle B, Milkowski K, Akram M, Pourkashanian M, Lucquiaud M. Flexible operation of post-combustion CO2 capture at pilot scale with demonstration of capture-efficiency control using online solvent measurements. Int J Greenh Gas Control 2018;71:253–77.
[7] Wilkes MD, Mukherjee S, Brown S. Transient CO2 capture for open-cycle gas turbines in future energy systems. Energy; 2021a. p. 119258.
[8] Rúa J, Bui M, Nord LO, Mac Dowell N. Does CCS reduce power generation flexibility? A dynamic study of combined cycles with post-combustion CO2 capture. Int J Greenh Gas Control 2020;95:102984.
[9] Bui M, Adjiman CS, Bardow A, Anthony EJ, Boston A, Brown S, Fennell PS, Fuss S, Galindo A, Hackett LA, Hallett JP, Harzog HJ, Jackson G, Kemper J, Krevor S, Maitland GC, Matuszewski M, Metcalfe IS, Petit C, Puxty G, Reimer J, Reiner D, Rubin E, Scott S, Shah N, Smit B, Trusler JP, Webley P, Wilcox J, Mac Dowell N. Carbon capture and storage (CCS): the way forward. Energy Environ Sci 2018;11(5):1062–176.
[10] Chao C, Deng Y, Dewil R, Baeyens J, Fan X. Post-combustion carbon capture. Renew Sustain Energy Rev 2021;138:110490.
[11] Li J-R, Ma Y, McCarthy MC, Sculley J, Yu J, Jeong H-K, Balbuena PB, Zhou H-C. Carbon dioxide capture-related gas adsorption and separation in metal-organic frameworks. Coord Chem Rev 2011;225(16):1791–823.
[12] Samanta A, Zhao A, Shimizu GKH, Sarkar P, Gupta R. Post-combustion CO2 capture using solid sorbents: a review. Ind Eng Chem Res 2012;51:1438–63.
[13] Ben-Mansour R, Habib MA, Bamidele OE, Basha M, Qasem NAA, Peedikakkal A, Laoui T, Ali M. Carbon capture by physical adsorption: materials, experimental investigations and numerical modeling and simulations – a review. Appl Energy 2016;161:225–55.
[14] Song C, Liu Q, Ji N, Deng S, Zhao J, Li Y, Song Y, Li H. Alternative pathways for efficient CO2 capture by hybrid processes—a review. Renew Sustain Energy Rev 2018;82(1):215–31.
[15] Zanco SE, Joss L, Hefti M, Gazzani M, Mazzotti M. Addressing the criticalities for the deployment of adsorption-based CO2 capture processes. Energy Proc 2017;114:2497–505.
[16] Clausse M, Merel J, Meunier F. Numerical parametric study on CO2 capture by indirect thermal swing adsorption. Int J Greenh Gas Control 2011;5(5):1206–13.
[17] Wang L, Liu Z, Li P, Yu J, Rodrigues AE. Experimental and modelling investigation on post-combustion carbon dioxide capture using zeolite 13X-APG by hybrid VTSA process. Chem Eng J 2012;197:151–61.
[18] Wang L, Yang Y, Shen W, Kong X, Li P, Yu J, Rodrigues AE. CO2 capture from flue gas in an existing coal-fired power plant by two successive pilot-scale VPSA units. Ind Eng Chem Res 2013;52(23):7947–55.
[19] Ghougassian PG, Lopez JAP, Manousiouthakis VI, Smirniotis P. CO2capturing from power plant flue gases: energetic comparison ofamine absorption with MgO based, heat integrated,pressure–temperature-swing adsorption. Int J Greenh Gas Control 2014;22:256–71.
[20] Plaza MG, Rubiera F. Development of carbon-based vacuum, temperature and concentration swing adsorption post-combustion CO2 capture processes. Chem Eng J 2019a;375:122002.
[21] Zhao W, Zhang Z, Li Z, Cai N. Continuous CO2 capture in dual fluidized beds using silica supported amine. Energy Proc 2013;37:89–98.
[22] Pröll T, Schöny G, Sprachmann G, Hofbauer H. Introduction and evaluation of a double loop staged fluidized bed system for post-combustion CO2 capture using solid sorbents in a continuous temperature swing adsorption process. Chem Eng Sci 2016;141:166–74.
[23] Schöny G, Dietrich F, Fuchs J, Pröll T, Hofbauer H. A multi-stage fluidized bed system for continuous CO2 capture by means of temperature swing adsorption – first results from bench scale experiments. Powder Technol 2017;316:519–27.
[24] Kim K, Park Y-K, Park J, Jung E, Seo H, Kim H, Lee KS. Performance comparison of moving and fluidized bed sorption systems for an energy-efficient solid sorbent-based carbon capture process. Energy Proc 2014;63:1151–61.
[25] Grande CA, Kvamsdal H, Mondino G, Blom R. Development of moving bed temperature swing adsorption (MBTSA) process for post-combustion CO2 capture: initial benchmarking in a NGCC context. Energy Proc 2017;114:2203–10.
[26] Mondino G, Grande CA, Blom R, Nord LO. Moving bed temperature swing adsorption for CO2 capture from a natural gas combined cycle power plant. Int J Greenh Gas Control 2019;85:58–70.
[27] Jiang N, Shen Y, Liu B, Zhang D, Tang Z, Li G, Fu B. CO2 capture from dry flue gas by means of VPSA, TSA and TVSA. J CO2 Util 2020;35:153–68.
[28] Yang H, Fan S, Lang X, Wang Y, Nie J. Economic comparison of three gas separation technologies for CO2 capture from power plant flue gas. Chin J Chem Eng 2011;19(4):615–20.
[29] Liu Z, Wang L, Kong X, Li P, Yu J, Rodrigues AE. Onsite CO2 capture from flue gas by an adsorption process in a coal-fired power plant. Ind Eng Chem Res 2012;51:7355–63.
[30] Shen C, Liu Z, Li P, Yu J. Two-stage VPSA process for CO2 capture from flue gas using activated carbon beads. Ind Eng Chem Res 2012;51(13):5011–21.
[31] Zhao R, Deng S, Zhao L, Zhao Y, Li S, Zhang Y, Yu Z. Experimental study and energy-efficiency evaluation of a 4-step pressure-vacuum swing adsorption (PVSA) for CO2 capture. Energy Convers Manag 2017;151:179–89.
[32] Nikolaidis GN, Kikkinides ES, Georgiadis MC. Modelling and optimization of pressure swing adsorption (PSA) processes for post-combustion CO2 capture from flue gas. In: Papadopoulos AI, Seferlis P, editors. Process systems and materials for CO2 capture. John Wiley & Sons Ltd; 2017a. p. 343–69.
[33] Luberti M, Oreggioni GD, Ahn H. Design of a rapid vacuum pressure swing adsorption (RVPSA) process for post-combustion CO2 capture from a biomass-fuelled CHP plant. J Environ Chem Eng 2017;5(4):3973–82.
[34] Xing R, Shi W, Shen Y, Liu B, Zhang D. Vacuum pressure swing adsorption system for N2/CO2 separation in consideration of unstable feed concentration. Adsorption 2019;25:1147–58.
[35] Ishibashi M, Ota H, Akutsu N, Umeda S, Tajika M, Izumi J, Yasutake A, Kabata T, Kageyama Y. Technology for removing carbon dioxide from power plant flue gas by the physical adsorption method. Energy Convers Manag 1996;37(6–8):929–33.
[36] Merel J, Clausse M, Meunier F. Experimental investigation on CO2 Post–Combustion capture by indirect thermal swing adsorption using 13X and 5A zeolites. Ind Eng Chem Res 2008;47(1):209–15.
[37] Zhang J, Webley PA, Xiao P. Effect of process parameters on power requirements of vacuum swing adsorption technology for CO2 capture from flue gas. Energy Convers Manag 2008;49(2):346–56.
[38] Krishnamurthy S, Rao VR, Guntuka S, Sharratt P, Haghpanah R, Rajendran A, Amanullah M, Karimi IA, Farooq S. CO2 capture from dry flue gas by vacuum swing adsorption: a pilot plant study. AIChE J 2014;60(5):1830–42.
[39] Wawrzyńczak D, Majchrzak-Kucęba I, Srokosz K, Kozak M, Nowak W, Zdeb J, Smółka W, Zajchowski A. The pilot dual-reflux vacuum pressure swing adsorption unit for CO2 capture from flue gas. Separ Purif Technol 2019;31:560–70.
[40] Chue KT, Kim JN, Yoo YJ, Cho SH, Yang RT. Comparison of activated carbon and zeolite 13X for CO2 recovery from flue gas by pressure swing adsorption. Ind Eng Chem Res 1995;34(2):591–8.
[41] Diagne D, Goto M, Hirose T. Numerical analysis of a dual refluxed PSA process during simultaneous removal and concentration of carbon dioxide dilute gas from air. J Chem Technol Biotechnol 1996;65(1):29–38.
[42] Ding Y, Alpay E. Equilibria and kinetics of CO2 adsorption on hydrotalcite adsorbent. Chem Eng Sci 2000;55(17):3461–73.
[43] Choi W-K, Kwon T-I, Yeo Y-K, Lee H, Song HK, Na B-K. Optimal operation of the pressure swing adsorption (PSA) process for CO2 recovery. Kor J Chem Eng 2003;20(4):617–23.
[44] Chou C-T, Chen C-Y. Carbon dioxide recovery by vacuum swing adsorption. Separ Purif Technol 2004;39(1–2):51–65.
[45] Ko D, Siriwardane R, Biegler LT. Optimization of pressure swing adsorption and fractionated vacuum pressure swing adsorption processes for CO2 capture. Ind Eng Chem Res 2005;44:8084–94.
[46] Agarwal A. "'Advanced strategies for optimal design and operation of pressure swing adsorption Processes',PhD thesis,". Pittsburgh: Carnegie Mellon University; 2010.
[47] Dantas TLP, Luna FMT, , I. J. S. Jr., Azevedo DC Sd, Grande CA, Rodrigues AE, Moreira RFPM. Carbon dioxide–nitrogen separation through adsorption on

activated carbon in a fixed bed. Chem Eng J 2011a;169(1–3):11–9.
[48] Dantas TLP, Luna FMT, , I. J. S. Jr., Torres AEB, Azevedo DC Sd, Grande CA, Rodrigues AE, Moreira RFPM. Modeling of the fixed-bed adsorption of carbon dioxide and a carbon dioxide- nitrogen mixture on zeolite 13X. Braz J Chem Eng 2011b;28(3):533–44.
[49] Dantas TLP, Luna FMT, , I. J. S. Jr., Torres AEB, Azevedo DC Sd, Grande CA, Rodrigues AE, Moreira RFPM. Carbon dioxide–nitrogen separation through pressure swing adsorption. Chem Eng J 2011c;172(2–3):698–704.
[50] Krishna R, Long JR. Screening metal-organic frameworks by analysis of transient breakthrough of gas mixtures in a fixed bed adsorber. J Phys Chem C 2011;115(26):12941–50.
[51] Krishna R, Baten JMv. A comparison of the CO2 capture characteristics of zeolites and metal–organic frameworks. Separ Purif Technol 2012;87:120–6.
[52] Mulgundmath VP, Jones R, Tezel FH, Thibault J. Fixed bed adsorption for the removal of carbon dioxide from nitrogen: breakthrough behaviour and modelling for heat and mass transfer. Separ Purif Technol 2012;85:17–27.
[53] Ribeiro RPPL, Grande CA, Rodrigues AE. Activated carbon honeycomb monolith – zeolite 13X hybrid system to capture CO2 from flue gases employing Electric Swing Adsorption. Chem Eng Sci 2013;104:304–18.
[54] Haghpanah R, Nilam R, Rajendran A, Farooq S, Karimi IA. Cycle synthesis and optimization of a VSA process for postcombustion CO2 capture. AIChE J 2013a;59(12):4735–48.
[55] Riboldi L, Bolland O. Evaluating Pressure Swing Adsorption as a CO2 separation technique in coal-fired power plants. Int J Greenh Gas Control 2015;39:1–16.
[56] Horstmeier JF, Lopez A, Agar D. Performance improvement of vacuum swing adsorption processes for CO2 removal with integrated phase change material. Int J Greenh Gas Control 2016;47:364–75.
[57] Plaza MG, Durán I, Querejeta N, Rubiera F, Pevida C. Experimental and simulation study of adsorption in postcombustion conditions using a microporous biochar. 1. CO2 and N2 adsorption. Ind Eng Chem Res 2016a;55(11):3097–112.
[58] Plaza MG, Durán I, Querejeta N, Rubiera F, Pevida C. Experimental and simulation study of adsorption in postcombustion conditions using a microporous biochar. 2. H2O, CO2, and N2 adsorption. Ind Eng Chem Res 2016b;55(24):6854–65.
[59] Nikolaidis GN, Kikkinides ES, Georgiadis MC. An integrated two-stage P/VSA process for postcombustion CO2 capture using combinations of adsorbents zeolite 13X and MgMOF-74. Ind Eng Chem Res 2017b;56(4):974–988.
[60] Plaza MG, Rubiera F, Pevida C. Evaluating the feasibility of a TSA process based on steam stripping in combination with structured carbon adsorbents to capture CO2 from a coal power plant. Energy Fuel 2017;31(9):9760–75.
[61] Zarghampoor MH, Mozaffarian M, Soleimani M, Ravanchi MT. Modeling of CO2 adsorption on activated carbon and 13X zeolite via vacuum swing adsorption. IOP Conf Ser Mater Sci Eng 2017;206.
[62] Li S, Deng S, Zhao L, Zhao R, Lin M, Du Y, Lian Y. Mathematical modeling and numerical investigation of carbon capture by adsorption: literature review and case study. Appl Energy 2018;221:437–49.
[63] Ben-Mansour R, Qasem NAA, Antar MA. Carbon dioxide adsorption separation from dry and humid CO2/N2 mixture. Carbon dioxide adsorption separation from dry and humid CO2/N2 mixture 2018;117:221–35.
[64] Lillia S, Bonalumi D, Grande C, Manzolini G. A comprehensive modeling of the hybrid temperature electric swingadsorption process for CO2 capture. Int J Greenh Gas Control 2018;74:155–73.
[65] Qasem NAA, Ben-Mansour R. Adsorption breakthrough and cycling stability of carbon dioxide separation from CO2/N2/H2O mixture under ambient conditions using 13X and Mg-MOF-74. Appl Energy 2018;230:1093–107.
[66] Goyal P, Purdue MJ, Farooq S. Adsorption and diffusion of N2 and CO2 and their mixture on silica gel. Ind Eng Chem Res 2019;58(42):19611–22.
[67] Xu M, Chen S, Seo D, Deng S. Evaluation and optimization of VPSA processes with nanostructured zeolite NaX for post-combustion CO2 capture. Chem Eng J 2019;371:693–705.
[68] Ahn H, Hong S-H, Zhang Y, Lee C-H. Experimental and simulation study on CO2 adsorption dynamics of a zeolite 13X column during blowdown and pressurization: implications of scaleup on CO2 capture vacuum swing adsorption cycle. Ind Eng Chem Res 2020;59(13):6053–64.
[69] Tian J, Shen Y, Zhang D, Tang Z. CO2 capture by vacuum pressure swing adsorption from dry flue gas with a structured composite adsorption medium. J Environ Chem Eng 2021;9:106037.
[70] Boscherinia M, Miccio F, Papa E, Medri V, Landi E, Doghieri F, Minelli M. The relevance of thermal effects during CO2 adsorption and regeneration in a geopolymer-zeolite composite: experimental and modelling insights. Chem Eng J 2021;408:127315.
[71] Kikkinides ES, Nikolic D, Georgiadis MC. Modeling of pressure swing adsorption processes. In: Georgiadis MC, Banga JR, Pistikopoulos EN, editors. Dynamic process modelling. Weinheim, Germany, Wiley-VCH Verlag GmbH & Co. KGaA; 2010. p. 137–72.
[72] Ruthven DM. Principles of adsorption and adsorption processes. John Wiley & Sons; 1984. p. 206–19.
[73] Plaza MG, Rubiera F. Evaluation of a novel multibed heat-integrated vacuum and temperature swing adsorption post-combustion CO2 capture process. Appl Energy 2019b;250:916–25.
[74] Glueckauf E, Coates JI. 241. Theory of chromatography. Part IV. The influence of incomplete equilibrium on the front boundary of chromatograms and on the effectiveness of separation. J Chem Soc 1947:1315–21.
[75] Xiao P, Zhang J, Webley P, Li G, Singh R, Todd R. Capture of CO2 from flue gas streams with zeolite 13X by vacuum-pressure swing adsorption. Adsorption 2008;14:575–82.
[76] Haghpanah R, Majumder A, Nilam R, Rajendran A, Farooq S, Karimi IA, Amanullah M. Multiobjective optimization of a four-step adsorption process for postcombustion CO2 capture via finite volume simulation. Ind Eng Chem Res 2013b;52(11):4249–65.
[77] Chue KT, Kim JN, Yoo YJ, Cho SH, Yang RT. Comparison of activated carbon and zeolite 13X for CO2 recovery from flue gas by pressure swing adsorption. Ind Eng Chem Res 1995;34:591–8.
[78] Ergun S. Determination of geometric surface area of crushed porous solids. Anal Chem 1952;24:388–93.
[79] PSE. gPROMS ProcessBuilder documentation. London: Process Systems Enterprise Limited; 2019.
[80] Li D, Zhou Y, Shen Y, Sun W, Fu Q, Yan H, Zhang D. Experiment and simulation for separating CO2/N2 by dual-reflux pressure swing adsorption process. Chem Eng J 2016;297:315–24.
[81] Moon D-K, Park Y, Oh H-T, Kim S-H, Oh M, Lee C-H. Performance analysis of an eight-layered bed PSA process for H2 recovery from IGCC with pre-combustion carbon capture. Energy Convers Manag 2018;156:202–14.
[82] Solares RAA, Santos DSd, Ingram A, Wood J. Modelling and parameter estimation of breakthrough curves for amine-modified activated carbons under pre-combustion carbon capture conditions. Fuel 2019;253:1130–9.
[83] McGaughey AJH, Kaviany M. Thermal conductivity decomposition and analysis using molecular dynamics simulations: Part II. Complex silica structures. Int J Heat Mass Tran 2004;47(8–9):1799–816.
[84] Engineering ToolBox. Ratios of specific heat of gase [Online]. Available: https://www.engineeringtoolbox.com/specific-heat-ratio-d_608.html. [Accessed 25 October 2021].
[85] Khoramzadeh E, Mofarahi M, Lee C-H. Equilibrium adsorption study of CO2 and N2 on synthesized zeolites 13X, 4A, 5A, and beta. J Chem Eng Data 2019;64(12):5648–64.
[86] Wilkins NS, Rajendran A. Measurement of competitive CO2 and N2 adsorption on Zeolite 13X for post-combustion CO2 capture. Adsorption 2019;25:115–33.
[87] Webley PA. Adsorption technology for CO2 separation and capture: a perspective. Adsorption 2014;20:225–31.
[88] Energiewende Agora. Flexibility in thermal power plants. Berlin: Agora Energiewende; 2017.
[89] ELEXON. Generation by fuel type [Online]. Available: https://www.bmreports.com/bmrs/?q=generation/fueltype. [Accessed 1 April 2019].
[90] He Z, Sahraei MH, Ricardez-Sandoval LA. Flexible operation and simultaneous scheduling and control of a CO2 capture plant using model predictive control. Int J Greenh Gas Control 2016;48(Part 2):300–11.
[91] Patrón GD, Ricardez-Sandoval L. An integrated real-time optimization, control, and estimation scheme for post-combustion CO2 capture. Appl Energy 2022;308:118302.
[92] Rúa J, Nord LO. Optimal control of flexible natural gas combined cycles with stress monitoring: linear vs nonlinear model predictive control. Appl Energy 2020;265:114820.
[93] Johnsen K, Helle K, Myhrvold T. Scale-up of CO2 capture processes: the role of Technology Qualification. Energy Proc 2009;1:163–70.
[94] I. PRAXAIR TECHNOLOGY. VPSA PROCESS and enhanced oxygen recovery. Patent WO 2008/005492 A1 10 January 2009.
[95] Stinn M, Vance J. Selecting valves for pressure swing adsorption. 2018. Emerson.
[96] Wilkes MD, Mukherjee S, Brown S. Linking CO2 capture and pipeline transportation: sensitivity analysis and dynamic study of the compression train. Int J Greenh Gas Control 2021b;111:103449.
[97] Wu X, Wang M, Liao P, Shen J, Li Y. Solvent-based post-combustion CO2 capture for power plants: a critical review and perspective on dynamic modelling, system identification, process control and flexible operation. Appl Energy 2020;257:113941.
[98] Du W, Alkebsi KAM. Model predictive control and optimization of vacuum pressure swing adsorption for carbon dioxide capture. In: 6th international symposium on advanced control of industrial processes; 2017. Taipei, Taiwan.
[99] Jung H, Heo S, Lee JH. Model predictive control for amine-based CO2 capture process with advanced flash stripper. Control Eng Pract 2021;114:104885.
[100] Rúa J, Hillestad M, Nord LO. Model predictive control for combined cycles integrated with CO2 capture plants. Comput Chem Eng 2021;146:107217.